JOC The Journal of Organic Chemistry

Note

pubs.acs.org/joc

Easily Reducible Materials from the Reactions of Diselenopheno[3,2-*b*:2′,3′-d]pyrrole and Dithieno[3,2-*b*:2′,3′-*d*]pyrrole with Tetracyanoethylene

Yulia A. Getmanenko,[†] Thomas A. Purcell,[‡] Do Kyung Hwang,[§,∥] Bernard Kippelen,[§] and Seth R. Marder*[,†]

[†]Department of Chemistry & Biochemistry, Center for Organic Photonics and Electronics, Georgia Institute of Technology, 901 Atlantic Drive NW, Atlanta, Georgia 30332-0400, United States

[‡]New York University, 100 Washington Square East, New York, New York 10003, United States

[§]School of Electrical and Computer Engineering, Center for Organic Photonics and Electronics, Georgia Institute of Technology, 777 Atlantic Drive NW, Atlanta, Georgia 30332-0250, United States

[∥]Interface Control Research Center, Future Convergence Research Division, Korea Institute of Science and Technology (KIST), Hwarangno 14-gil 5, Seongbuk-gu, Seoul 136-791, Korea

Supporting Information

ABSTRACT: A new core, 4*H*-diselenopheno[3,2-*b*:2′,3′-*d*]-pyrrole (DSP), was reacted with tetracyanoethylene, and three products, mono-tricyanovinyl, bis-tricyanovinyl, and quinoidal, were isolated and compared with the respective 4*H*-dithieno-[3,2-*b*:2′,3′-*d*]pyrrole (DTP) derivatives using cyclic voltammetry, UV−vis absorption, and differential scanning calorimetry analyses. Organic field-effect transistors were fabricated using solution-processed films, and only one derivative, bis-tricyanovinyl-DSP, exhibited transistor behavior with μ_e reaching 8.7×10^{-4} $cm^2/V{\cdot}s$. This enhancement of the electron-transporting properties in comparison with DTP derivative is attributed to stronger LUMO−LUMO interaction due to a larger size of selenium atom, which in the case of the bis-tricyanovinyl derivative, has wave function density on the chalcogen.

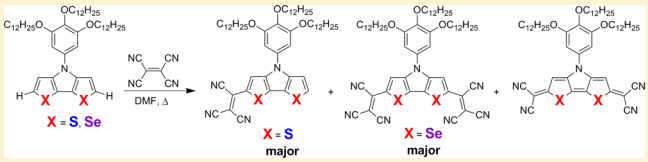

The development of solution-processable electron-transporting (ET) organic semiconductors for use in organic field-effect transistors (OFETs) that exhibit high mobility values and high current on−off ratios and stability in air and under electrical stress remains a challenging task; however, substantial progress in this field had been achieved in recent years.[1,2] The design of such materials typically includes planar aromatic cores functionalized with strong electron-withdrawing groups to increase the electron affinity (EA), thus facilitating charge injection. The tricyanovinyl (TCV) and dicyanovinylene (DCV) groups were explored in combination with various π-systems[3−10] to achieve high EA (which is often probed indirectly by electrochemistry). Rasmussen's group[11] reported the isolation of three products from the reaction of *N*-(*p*-hexylphenyl)-substituted 4*H*-dithieno[3,2-*b*:2′,3′-*d*]pyrrole (DTP) with tetracyanoethylene (TCNE), with two minor products, bis-TCV and quinoidal material, possessing large EA. The materials isolated were not particularly soluble, and no characterization in OFET devices was reported. Taking into consideration the ease of the first reduction of these compounds, the possibility for modification of the group at the nitrogen atom to improve the solubility and availability of the selenium analogue of DTP, 4*H*-diselenopheno[3,2-*b*:2′,3′-*d*]pyrrole (DSP),[12] we decided to investigate the products of reaction of TCNE with DTP and DSP as potential ET materials.

The influence of the nature of chalcogen on the charge transport behavior of the related cores was reported by Handa et al., wherein they examined dicyanomethylene quinoidal derivatives with terthiophene[13] and mixed[14] skeleton in solution-processed OFETs. It was found that substitution of sulfur with selenium led to one order magnitude decrease in electron mobility μ_e and enhanced hole mobility μ_h, which was attributed to the wave function distribution (chalcogen has a very little contribution to LUMOs and substantial contribution to HOMOs, and as a result larger size of selenium can only enhance the hole transport).

SYNTHESIS

Starting materials **2** were obtained from their respective 2,7-bis-trimethylsilyl derivatives[12] **1** by the reaction with tetra-*n*-butylammonium fluoride (TBAF) in 69% and 85% yield, respectively (Scheme 1). Material **2a** was also prepared in 60% yield using modified literature procedures[12,15] starting from 3,3′-dibromo-2,2′-dithiophene, which was prepared by the $CuCl_2$-oxidative coupling of 2-lithio-3-bromothiophene[16] generated from 3-bromothiophene by the lithiation with lithium diisopropylamide at −78 °C. The reaction of **2a** with excess of

Received: September 17, 2012
Published: October 25, 2012

Scheme 1. Reaction DTP (2a) and DSP (2b) with TCNE

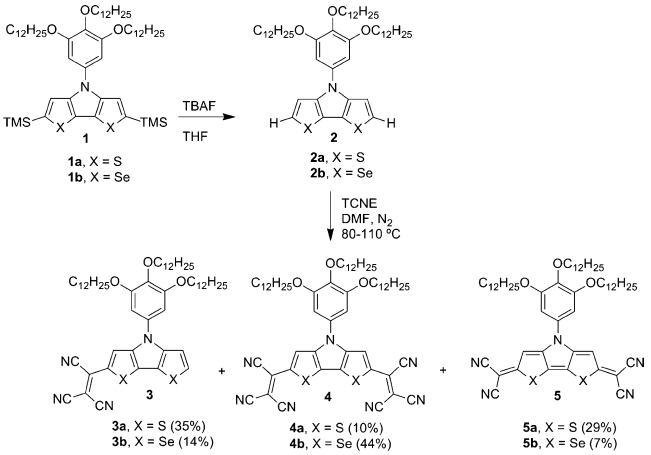

TCNE in DMF at 80 °C resulted in a mono-TCV product **3a** as a major material, and desired bis-TCV product **4a** and quinoidal product **5a** as two minor materials, as it was observed by Rasmussen's group.[11] Use of the excess of TCNE and/or increase of the reaction temperature (up to 110 °C) or time did not substantially improve the yield of **4a**. Surprisingly, the reaction of **2b** resulted in a different product distribution, and desired bis-TCV product **4b** was isolated as a major compound, while both mono- and quinoidal materials were obtained as minor products. It is not clear what accounts for such increased reactivity of the mono-TCV derivative with the second molecule of TCNE. While **1b** is somewhat easier to oxidize in comparison with **1a**,[12] which suggests that the DSP core is more electron-rich in comparison with DTP, the oxidation potentials of mono-TCV derivatives of DTP and DSP are quite similar (Table 1) with DSP derivative being the one that is slightly more difficult to oxidize. The reaction mechanism,[11] proposed for the formation of both mono- and bis-TCV DTP products, involves the electron-transfer reaction as a first step, and experimental results with DSP suggest that this step is more favorable for the selenium-containing core.

2. ELECTRONIC, ELECTROCHEMICAL, AND ELECTRICAL PROPERTIES OF 3–5

Solution UV–vis absorption spectra of DTP and DSP derivatives in dichloromethane have similar band structure; for **3b** and **4b**, absorption maxima are bathochromically shifted in comparison with the respective DTP derivatives (Figure 1, Table 1), while for quinoidal products **5** the position and the shape of the absorption band are strikingly similar. For all products, substitution of sulfur with selenium leads to increase of the extinction coefficient (by ~8% for **3b** and **5b**, and by ~13% for **4b**).

The film absorption spectra of **3** are quite similar, and the λ_{max} is hypsochromically shifted for both materials in comparison with their solution spectra. A much larger difference between the film absorption spectra of the DTP and DSP derivatives is observed for bis-TCV materials **4** and quinoidal products **5**. While the film absorption spectrum of **4a** shows a band with one maximum, a broader band with two maxima is observed for **4b** suggesting stronger intramolecular interaction. Band broadening is also observed upon the substitution of sulfur with selenium in quinoidal products **5**.

Electrochemical properties were examined by the cyclic voltammetry (CV) in two different solvents (Figure 2, Table 1). For mono-TCV derivatives **3** the first reduction potentials in dichloromethane are very similar, while in less polar solvent, tetrahydrofuran, both first and second reduction potentials for the DSP derivative **3b** are more negative (harder to reduce) (by 0.03 and 0.07 V, respectively) in comparison with the DTP derivative **3a**. For bis-TCV derivatives, DSP derivative **4b** is slightly more easy to reduce in dichloromethane with both first and second reduction potentials being more positive in comparison with **4a** (by 0.02 and 0.03 V, respectively), while in THF the first reduction potentials for **4a** and **4b** are identical, and the second reduction is easier for DTP derivative (by 0.04 V). For the quinoidal products **5** a somewhat similar trend is observed, when in dichloromethane the DSP derivative is easier to reduce (by 0.05 V), while in THF both first and second reduction potentials are more negative (harder to reduce) for both first and second reductions (by 0.07 and 0.08 V, respectively).

In comparison with the respective thiophene-based quinoidal material, 2,2′-(thiophene-2,5-diylidene)dimalononitrile,[17] and

Table 1. Summary of UV–vis Absorption and CV Analyses

entry	λ_{max}, nm ($\varepsilon \times 10^{-3}$, $M^{-1}cm^{-1}$) (CH_2Cl_2)	λ_{max} (film), nm	solvent for CV	$E_{1/2}^{0/1+}$, V[a]	$E_{1/2}^{0/1-}$, V[a]	$E_{1/2}^{1-/2-}$, V[a]	$E_{1/2}^{1-/2-}$-$E_{1/2}^{0/1-}$, V	$E_{1/2}^{0/1-}$, V^1 (vs SCE)[b]	EA, eV[c]
3a	284 (15.5), 536 (49.0)	519	CH_2Cl_2	+0.90	−0.96	−1.63	0.67	−0.50	−3.84
			THF	n/a	−0.96	−1.73	0.77	−0.40	
3b	363 (13.4), 549 (52.8)	512	CH_2Cl_2	+0.92	−0.97	−1.62	0.65	−0.51	−3.83
			THF	n/a	−1.00	−1.80	0.80	−0.44	
4a	267 (17.1), 374 (10.5), 576 (78.7)	550	CH_2Cl_2	n/a	−0.51	−0.81	0.30	−0.05	−4.29
			THF	n/a	−0.54	−0.85	0.31	+0.02	
4b	276 (17.8), 383 (10.4), 596 (88.7)	529, 610	CH_2Cl_2	+1.02[d]	−0.49	−0.78	0.29	−0.03	−4.31
			THF	n/a	−0.54	−0.89	0.35	+0.02	
5a	375 (8.96), 509 (75.2), 546 (96.4)	514	CH_2Cl_2	+1.06	−0.66	−0.96	0.30	−0.20	−4.14
			THF	n/a	−0.62	−1.02	0.40	−0.06	
5b	276 (10.5), 510 (79.5), 547 (104.0)	549	CH_2Cl_2	+1.06	−0.61	−0.96	0.34	−0.13	−4.11
			THF	n/a	−0.69	−1.10	0.41	−0.09	

[a]0.1 M $^nBu_4NPF_6$, in the specified solvent, Cp_2Fe internal standard at 0 V, 50 $mV{\cdot}s^{-1}$ scan rate. [b]Potentials were estimated vs SCE using the following formula: $E_{1/2}^{0/1-}$(vs SCE) = $E_{1/2}^{0/1-}$(vs Cp_2Fe) + 0.56 (V) (for THF); $E_{1/2}^{0/1-}$(vs SCE) = $E_{1/2}^{0/1-}$(vs Cp_2Fe) + 0.46 (V) (for CH_2Cl_2).[18] [c]Electron affinity EA was estimated as follows: EA = $-(eE_{1/2}^{0/-} + 4.8$ eV).[19] [d]For **4b** oxidation at +1.02 V is not reversible (large error).

dx.doi.org/10.1021/jo3020006 | J. Org. Chem. 2012, 77, 10931–10937

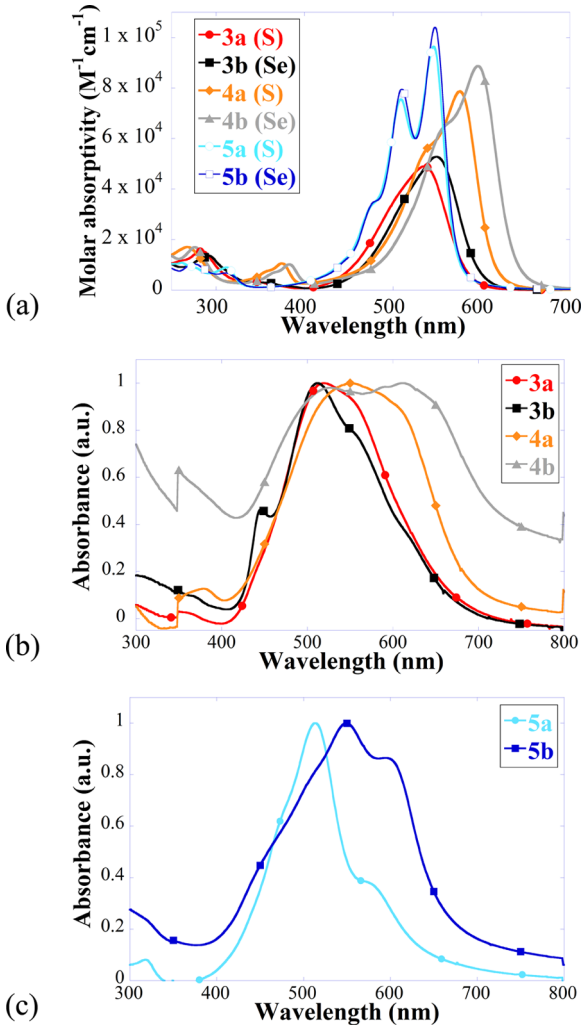

Figure 1. UV–vis absorption spectra of **3**–**5**: (a) in dichloromethane; (b, c) as neat films.

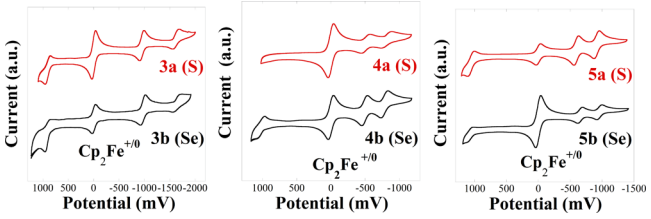

Figure 2. Cyclic voltammetry analyses (0.1 M of $^nBu_4PF_6$ in dichloromethane, $Cp_2Fe^{0/+}$ as internal reference at 0 V, 50 mV·s^{-1} scan rate).

selenophene-based quinoidal material, 2,2′-(selenophene-2,5-diylidene)dimalononitrile,[17] the difference between the first and second reduction potentials for quinoidal derivatives **5** is smaller (0.30–0.40 V (**5a**) vs 0.60 V;[17] and 0.34–0.41 V (**5b**) vs 0.51 V[17]), indicating reduced Coulombic repulsion in dianions due to delocalization over a larger (in comparison with thiophene and selenophene) π-systems of DTP and DSP.

DFT calculations (B3LYP/6-31G**) were performed to investigate the electronic structure of DTP and DSP derivatives. As it was observed for mono-TCV derivative of quaterthiophene,[20] the LUMOs of **3** are more localized on the TCV group with some coefficients on one of the chalcogens (closer to TCV-group) (Figure S4, Supporting Information), while HOMOs of **3** are delocalized over the π-system with the node on nitrogen and no contribution from trialkoxyphenyl substituent or chalcogen. This wave function distribution suggests that substitution of sulfur with selenium might lead to improved electron transport, but no benefit of having selenium is expected for the hole charge transport. For bis-TCV derivatives **4**, LUMOs are delocalized over the π-system with some coefficients on chalcogens, and the larger size of the selenium atom might contribute to improved electron charge transport in DSP derivative **4b** (vide infra). For quinoidal products **5** both HOMOs and LUMOs are delocalized over the π-system and dicyanomethylene groups, and while there is some chalcogen contribution observed for the HOMOs, there is no such contribution to the LUMOs, and enhancement of the electron transport due to larger selenium atom is not to be expected.

Differential scanning calorimetry (DSC) analysis of **3** and **4** showed two transitions (during both heating and cooling on the second cycle), while quinoidal products **5** showed more complex thermal behavior with three transitions observed for **5a** and four transitions observed for **5b** (Figure 3). For all DSP derivatives the temperatures for transition to isotropic liquid is

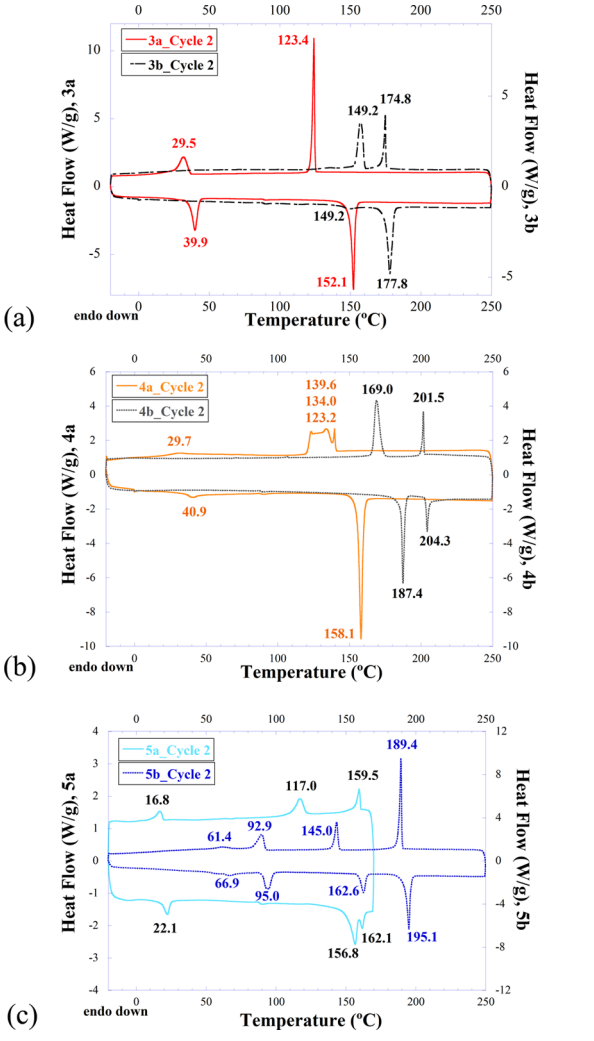

Figure 3. DSC analysis (second heating–cooling cycle, 10 °C/min heating and cooling rate): (a) mono-TCV derivatives **3**; (b) bis-TCV derivatives **4**; (c) quinoidal derivatives **5**.

dx.doi.org/10.1021/jo3020006 | J. Org. Chem. 2012, 77, 10931–10937

higher than that of DTP derivatives, providing further evidence for enhanced intermolecular interaction in the solid state.

Polarized optical microscopy (POM) analysis of **3b** showed the formation of a mesophase with the texture characteristic for Col_h phase followed by the transition to crystalline phase (Figure 4b), while **3a** formed the crystalline phase directly from the isotropic liquid (Figure 4a).

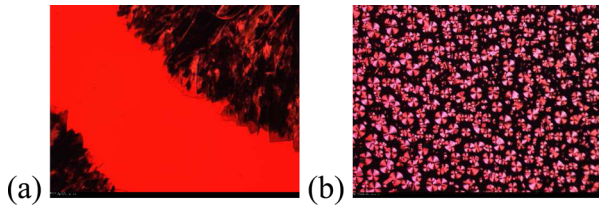

Figure 4. (a) Micrograph of **3a**, transition from isotropic liquid to crystalline phase, 149.7 °C. (b) POM micrograph of **3b**, spherulitic texture with maltese crosses of the mesophase formed from the isotropic liquid at 180.3 °C (image size ~870 × 650 μm).

Material **4a** forms an unidentified transient liquid crystalline phase (Figure 5a), followed by crystallization (Figure 5b). DSC

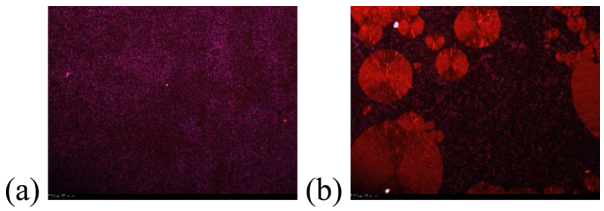

Figure 5. POM micrographs of **4a**: (a) 144.9 °C, not identified LC phase; (b) 143.0 °C, transition from unidentified LC to crystal phase (image size ~870 × 650 μm).

analysis of **4b** suggested formation of the possibly liquid crystalline phase for wider temperature range, but it was difficult to obtain a good quality micrograph to identify the phase that forms from the isotropic liquid.

While product **5b** shows formation of the liquid crystalline phase from the isotropic liquid (Figure 6(b), the nature of the first phase that forms from the isotropic liquid of **5a** is less clear, and the grainy texture was observed by the POM (Figure 6a).

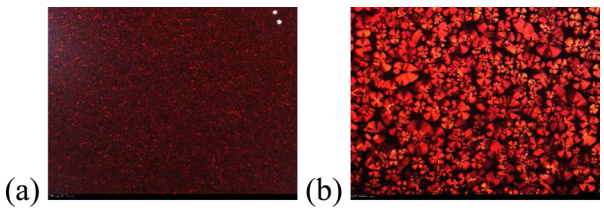

Figure 6. POM micrograph: (a) **5a**, 156.6 °C, not identified LC phase; (b) **5b**, 190.8 °C, formation of unidentified LC from the isotropic liquid (image size ~870 × 650 μm).

Materials **3**–**5** were tested in the *n*-channel OFETs (bottom gate, top contact configuration with Ca/Au electrodes) using solution-processed films, and devices fabricated with material **4b** were the only ones to show field-effect behavior (μ_e = 3.1 (±1.2) × 10^{-5} cm^2/V·s, V_{th} = −4.5 ± 3.6 V, I_{on}/I_{off} = 10) (Figure 7, Table S1, Supporting Information). This material was then tested in the top gate bottom contact device

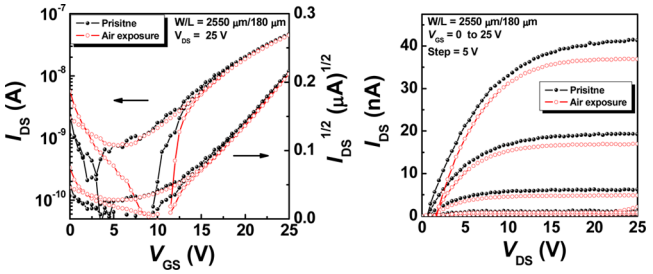

Figure 7. (Left) Transfer and (right) output characteristics of *n*-channel bottom-contact top-gate OFET of **4b** as active layer and CYTOP (45 nm)/Al_2O_3 (50 nm) dielectric layer with Au source/drain electrodes.

configuration using CYTOP (45 nm)/Al_2O_3 (50 nm) dielectric and gold electrodes,[9] and slight improvement in the device characteristics was observed with μ_e reaching 8.7 × 10^{-4} cm^2/V·s (V_{th} = 10.4 V, I_{on}/I_{off} = 50).

The device was exposed to ambient conditions for 9 months, and its characteristics (μ_e = 7.8 (±1.6) × 10^{-4} cm^2/V·s, V_{th} = 10.3 ± 0.9 V, I_{on}/I_{off} = 50) remained almost the same providing some evidence for good device stability.

In conclusion, we have tested 4-(3,4,5-tris(dodecyloxy)-phenyl)-4*H*-diselenopheno[3,2-*b*:2′,3′-*d*]pyrrole in the reaction with TCNE, and this core was found to have increased reactivity in comparison with dithieno[3,2-*b*:2′,3′-*d*]pyrrole, which resulted in the formation of the bis-tricyanovinyl derivative as a major product. This product was the only material with measurable electron mobility in *n*-channel OFET, suggesting that substitution of sulfur with selenium might lead to stronger intermolecular interaction and improved charge transport without significant change in the electrochemical and optical properties.

EXPERIMENTAL SECTION

General Methods. Anhydrous *N*,*N*-dimethylformamide (DMF) was used as received, and TCNE was sublimed prior to use. Tetrahydrofuran (THF) was distilled from sodium benzophenone ketyl. ^1H and $^{13}C\{^1H\}$ and DEPT-135 NMR spectra were acquired in $CDCl_3$ (peaks in ^1H NMR were referenced to solvent peak or tetramethylsilane at δ 0.00 ppm). UV−vis absorption spectra were recorded in 1 cm quarts cells. The solid-state UV−vis absorption was measured for the films prepared on the glass substrates using chlorobenzene solutions with concentration of ~10 mg/mL. DSP derivatives **3b** and **5b** were not completely dissolved at this concentration at room temperature, and the solutions were heated prior to filtration through 0.2 μm filter (for **5b** precipitation started before the spin-coating). Cyclic voltammetry (CV) experiments were carried out under nitrogen on dry deoxygenated dichloromethane or THF solutions *ca.* 10^{-4} M of analyte and 0.1 M solution of tetra-*n*-butylammonium hexafluorophosphate at scan rates of 50 $mV{\cdot}s^{-1}$ using a potentiostat, a platinum auxiliary electrode, a glassy carbon working electrode, and a silver wire anodized in 1 M aqueous potassium chloride (a pseudoreference electrode). Potentials were referenced to ferrocenium/ferrocene ($Cp_2Fe^{0/1+}$) as an internal standard at 0 V. Polarizing microscope equipped with the CCD camera and the hot stage was used for microscopy analysis (200× magnification).

Fabrication and Characterization of Organic Field-Effect Transistors (OFETs). For bottom gate and top contact geometry, OFETs were fabricated on heavily *n*-doped silicon substrates (n^+-Si, as the gate electrode) with 200-nm-thick thermally grown SiO_2 as the gate dielectric. Ti/Au (10 nm/100 nm) metalization on the backside of the substrate was used to enhance the gate electrical contact. Prior to surface modification, the substrates were treated by O_2 plasma for 3 min to increase hydrophilicity of the SiO_2 surface. SiO_2 dielectric

dx.doi.org/10.1021/jo3020006 | J. Org. Chem. 2012, 77, 10931−10937

surface was then coated with a thin buffer layer of BCB (Cyclotene, Dow Chemicals) to provide a high-quality hydroxyl-free interface (the solution of BCB in trimethylbenzene (TMB) with a ratio of 1:20 was spin coated at 3000 rpm for 60 s to provide a very thin uniform layer; thickness was not measured, final capacitance density was measured). The samples were cross-linked at 250 °C on a hot plate for 1 h in a N_2-filled glovebox. The total capacitance density (C_i) measured from parallel-plate capacitors was ∼13.8 nF/cm^2. The organic semiconductor layer of compound **4b** was formed on the substrates by spin coating a solution prepared from chlorobenzene (10 mg/mL) at 500 rpm for 10 s and at 2000 rpm for 20 s. Finally, Ca/Au source/drain electrodes were deposited by thermal evaporation through a shadow mask. Devices were never exposed to normal ambient during the process.

For top gate and bottom contact geometry, OFETs were fabricated on glass substrates (Corning Eagle^{2000}). Au (50 nm) bottom contact source/drain electrodes were deposited by thermal evaporation through a shadow mask. The organic semiconductor layer of **4b** compound was formed on the substrates by spin coating a solution prepared from chlorobenzene (30 mg/mL) at 500 rpm for 10 s and at 2000 rpm for 20 s. A CYTOP (45 nm)/Al_2O_3 (50 nm) bilayer[9] was used as top gate dielectric. The CYTOP solution (CTL-809M) was purchased from Asahi Glass with a concentration of 9 wt %. To deposit the 45-nm-thick CYTOP layer, the original solution was diluted with solvent (CT-solv.180) to have a solution:solvent volume ratio of 1:3.5. The CYTOP layers were then deposited by spin coating at 3000 rpm for 60 s. Samples were annealed at 100 °C for 10 min. Al_2O_3 (50 nm) films were deposited on CYTOP layers by atomic layer deposition (ALD) at 110 °C using alternating exposures of trimethyl aluminum and H_2O vapor at a deposition rate of approximately 0.1 nm per cycle. All spin-coating and annealing processes were carried out in a N_2-filled drybox. Finally, Al (150 nm) gate electrodes were deposited by thermal evaporation through a shadow mask.

All current−voltage (I−V) and capacitance−voltage (C−V) characteristics were measured in a N_2-filled glovebox (O_2, H_2O < 0.1 ppm) with an Agilent E5272A source/monitor unit and an Agilent 4284A LCR meter.

*4-(3,4,5-Tris(dodecyloxy)phenyl)-4H-dithieno[3,2-b:2′,3′-d]-pyrrole (**2a**).* 2,6-Bis(trimethylsilyl)-4-(3,4,5-tris(dodecyloxy)phenyl)-4*H*-dithieno[3,2-*b*:2′,3′-*d*]pyrrole (**1a**) (3.00 mmol, 2.85 g) was dissolved in THF (40 mL), and tetra-*n*-butylammonium fluoride (TBAF) (1.0 M in THF, 6.00 mmol, 6.0 mL) was added dropwise at room temperature under nitrogen atmosphere. The reaction mixture was stirred for ∼0.5 h, and the reaction completion was confirmed by TLC analysis (hexanes/dichloromethane (1:1) as eluant). Reaction mixture was treated with water, the organic phase was separated, and the aqueous phase was extracted with hexanes two times. The combined organic phases were dried over anhydrous magnesium sulfate, the drying agent was filtered off, and the organic solvents were removed by rotary evaporation. Crude product was purified by column chromatography (silica gel dichloromethane/hexanes (2:1), and then dichloromethane/ethyl acetate (10:1) as eluants). Combined fractions were subjected to rotary evaporation, the residue was dried under vacuum, and the product (**2a**) was obtained as yellowish solid (1.68 g, 69.2% yield). ^{1}H NMR (400 MHz, $CDCl_3$): δ 7.18 (appears as s, 4H), 6.78 (s, 2H), 4.02 (m, 6H), 1.85 (m, 6H), 1.63 (m, (6H), 1.45−1.20 (m, 48H), 0.91 (m, 9H). ^{13}C{^{1}H} NMR (400 MHz, $CDCl_3$): δ 153.7, 144.1, 136.4, 135.2, 123.3 (CH), 116.5, 112.2 (CH), 101.7 (CH), 73.6 (CH_2), 69.3 (CH_2), 31.9 (CH_2), 31.9 (CH_2), 30.4 (CH_2), 29.8 (CH_2), 29.7 (CH_2), 29.64 (CH_2), 29.6 (CH_2), 29.4 (CH_2), 29.36 (CH_2), 29.32 (CH_2), 26.2 (CH_2), 26.1 (CH_2), 22.7 (CH_2), 14.1 (CH_3) (expected number of alkyl carbon resonances is 24; only 16 resonances were observed presumably due to overlap) (assignment of the CH, CH_2 and CH_3 carbons was made based on DEPT-135 experiment) (^{1}H and ^{13}C{^{1}H} NMR recorded in $CDCl_3$ are in good agreement with the literature analyses reported in CD_2Cl_2).[15]

3,3′-Dibromo-2,2′-dithiophene. Lithium diisopropylamide (LDA) was prepared by the addition of *n*-butyllithium (2.89 M in hexanes, 0.100 mol, 84 mL) to a solution of diisopropylamine (0.110 mol, 11.1 g) in 50 mL of anhydrous THF (−78 °C to room temperature). This LDA solution was added dropwise to a solution of 3-bromothiophene (0.100 mol, 16.30 g) in 100 mL of anhydrous THF cooled in acetone/dry ice bath (nitrogen atmosphere). After the solution was stirred for 5 min, precipitation was observed. The reaction mixture was stirred for 1 h, and $CuCl_2$ (1.05 equiv, 0.105 mol, 14.11 g) was added in one portion (exothermic reaction). The mixture became very dark (with blue hue) and then orange-brown with precipitation. The reaction mixture was allowed to warm to room temperature and treated with aqueous HCl, and the organic phase was removed. The aqueous phase was extracted with diethyl ether several times, the combined organic phases were dried over $MgSO_4$, the drying agent was filtered off, and the solvents were removed by rotary evaporation. Crude product was obtained as dark tan or brown solid (∼100% yield), and this material was purified by Kugelrohr distillation (200−215 °C/0.5−0.8 mmHg) to give off-white solid in 70−80% yields (11.3 g (70.0% yield); 13.13 g (81.1%); lower purified yield of the product (52.3%) was observed on a larger scale (200 mmol) with the workup that involved the filtration of the reaction mixture diluted with hexanes through silica gel pad using hexanes and then dichloromethane as eluant). ^{1}H NMR (400 MHz, $CHCl_3$): δ 7.42 (d, J = 5.4 Hz, 2H), 7.09 (d, J = 5.4 Hz, 2H) (this analysis is in agreement with the literature data[21]).

*Reaction of **2a** with TCNE.* 4-(3,4,5-Tris(dodecyloxy)phenyl)-4*H*-dithieno[3,2-*b*:2′,3′-*d*]pyrrole (**2a**) (3.0 mmol, 2.42 g) was dissolved in anhydrous DMF (30 mL), and TCNE (4.0 equiv, 12.0 mmol, 1.54 g) was added (nitrogen atmosphere). The solution changed color from colorless to yellow-brown, then reddish-brown, and then dark red-wine. After the solution was stirred for 20 min at room temperature, a purple-red suspension formed. TLC analysis (chloroform as eluant) showed consumption of the starting material, formation of monotricyanovinyl product **3a** as a major product, quinoidal product **5a** as minor product and trace amount of bis-tricyanovinyl product **4a**. An additional amount of anhydrous DMF (20 mL) was added to the thick suspension, and the reaction mixture was heated at 72 °C (bath temperature) for ∼1 h, then at 55 °C (bath temperature) for 15 h, and then at 100 °C (bath temperature), and then heating was extended for 2 more weeks (no significant progress was observed, and additional byproducts were detected upon reaction time extension). The reaction mixture was cooled to room temperature and treated with water, and the dark solid was separated by vacuum filtration, washed with water, and dried. This solid was dissolved in chloroform−dichloromethane mixture and dried over anhydrous magnesium sulfate, the drying agent was filtered off, and the solvents were removed to give crude product, which was column chromatographed (silica gel, chloroform as eluant). First fractions containing **3a** were combined, the solvent was removed by rotary evaporation, and the product **3a** was obtained as dark solid (1.57 g, 35% yield). This material can be recrystallized from 2-propanol. Next fractions (hot-pink) containing quinoidal product **5a** were combined, the solvent was removed, and dark solid was obtained (0.82 g, 29%). Fractions containing **4a** (slightly contaminated with **5a**) were collected next, the solvent was removed, and **4a** was obtained (0.29 g, 9.7%).

*Purification of **4a**.* Material **4a** (0.29 g) isolated from the crude reaction mixture was further purified by column chromatography (silica gel, dichloromethane; in dichloromethane **4a** comes out first followed by **5a**). Fractions containing **4a** with very minor contamination were subjected to rotary evaporation, and the residue was purified by column chromatography two more times (silica gel, dichloromethane as eluant). Pure material was obtained as very dark solid (0.11 g, 39% recovery). This material can be recrystallized from 2-propanol.

*Purification of **5a**.* Material **5a** (0.82 g) obtained from the crude reaction mixture after the first column chromatography was further purified (silica gel, dichloromethane as eluant). Major fractions containing **5a** were combined, the solvent was removed and dark solid was obtained (0.60 g, 73% recovery; contaminated fractions were kept separately). This material was further purified for mobility measurement by three successive column chromatographies (silica gel, dichloromethane as eluant). The solvent was removed from combined fractions, and the residue was recrystallized from distilled 2-propanol twice (0.114 g, 13.9% recovery).

dx.doi.org/10.1021/jo3020006 | J. Org. Chem. 2012, 77, 10931−10937

3a. ^{1}H NMR (400 MHz, $CDCl_3$): δ 8.04 (s, 1H), 7.66 (d, J = 5.4 Hz, 1H), 7.14 (d, J = 5.4 Hz, 1H), 6.69 (s, 2H), 4.05 (t, J = 6.5 Hz, 2H), 4.00 (t, J = 6.3 Hz, 4H), 1.83 (m, 6H), 1.53 (m, 6H), 1.40−1.20 (m, 48H), 0.90 (m, 9H). ^{13}C{^{1}H} NMR (400 MHz, $CDCl_3$): δ 154.2, 152.6, 145.4, 137.9, 134.5 (CH), 132.6, 132.05, 131.9, 129.8, 121.7 (broad, CH), 116.7, 113.5, 113.3, 112.9, 112.4 (CH), 102.1 (CH), 73.7 (CH_2), 69.5 (CH_2), 31.92 (CH_2), 31.89 (CH_2), 30.4 (CH_2), 29.75 (CH_2), 29.73 CH_2, 29.68 (CH_2), 29.63 (CH_2), 29.60 (CH_2), 29.37 (CH_2), 29.34 (CH_2), 29.26 (CH_2), 26.1 (CH_2), 26.0 (CH_2), 22.7 (CH_2), 14.1 (CH_3) (expected number of alkyl carbon resonances is 24; only 17 resonances were observed presumably due to overlap) (assignment of the CH, CH_2 and CH_3 carbons was made based on DEPT-135 experiment). HRMS (MALDI-TOF): calcd for $C_{55}H_{80}N_4O_3S_2$ 908.5672, found 908.5626. Anal. Calcd for $C_{55}H_{80}N_4O_3S_2$: C, 72.64; H, 8.87; N, 6.16. Found: C, 72.89; H, 8.71; N, 6.13.

4a. ^{1}H NMR (400 MHz, $CDCl_3$): δ 8.09 (s, 2H), 6.64 (s, 2H), 4.06 (t, J = 6.6 Hz, 2H), 3.99 (t, J = 6.4 Hz, 4H), 1.86 (m, 6H), 1.49 (m, 6H), 1.27 (s, 48H), 0.89 (m, 9H). ^{13}C{^{1}H} NMR (400 MHz, $CDCl_3$): δ 154.6, 149.2, 138.8, 137.2, 132.9, 131.2, 125.3, 121.1 (CH), 112.6, 112.1, 111.6, 102.2 (CH), 84.9, 73.8 (CH_2), 69.6 (CH_2), 31.93 (CH_2), 31.91 (CH_2), 30.4 (CH_2), 29.76 (CH_2), 29.74 (CH_2), 29.69 (CH_2), 29.65 (CH_2), 29.61 (CH_2), 29.39 (CH_2), 29.36 (CH_2), 29.24 (CH_2), 26.09 (CH_2), 26.02 (CH_2), 22.7 (CH_2), 14.1 (CH_3) (expected number of alkyl carbon resonances is 24; only 17 resonances were observed presumably due to overlap) (assignment of the CH, CH_2 and CH_3 carbons was made based on DEPT-135 experiment). HRMS (MALDI-TOF): calcd for $C_{60}H_{79}N_7O_3S_2$ 1009.5686; found 1009.5707. Anal. Calcd for $C_{60}H_{79}N_7O_3S_2$: C, 71.32; H, 7.88; N, 9.70. Found: C, 71.49; H, 7.86; N, 9.57.

5a. ^{1}H NMR(400 MHz, $CDCl_3$): δ 6.52 (s, 2H), 6.50 (s, 2H), 4.03 (t, J = 6.6 Hz, 4H), 3.98 (t, J = 6.4 Hz, 4H), 1.86 (m, 7H), 1.49 (m, 7H), 1.27 (s, 56H), 0.90 (t, J = 6.5 Hz, 9H). ^{13}C{^{1}H} NMR (400 MHz, $CDCl_3$): δ 174.1, 163.7, 154.5, 139.5, 129.5, 129.2, 112.6, 112.4, 104.4 (CH), 102.8 (CH), 73.9 (CH_2), 73.5, 69.7 (CH_2), 31.9 (CH_2), 30.4 (CH_2), 29.78 (CH_2), 29.72 (CH_2), 29.67 (CH_2), 29.63 (CH_2), 29.41 (CH_2), 29.38 (CH_2), 29.3 (CH_2), 26.1 (CH_2), 22.7 (CH_2), 14.1 (CH_3) (expected number of alkyl carbon resonances is 24; only 14 resonances were observed presumably due to overlap). MS (MALDI-TOF): calcd for ($C_{56}H_{79}N_5O_3S_2$ + H) 934.6, found 934.6. Anal. Calcd for $C_{56}H_{79}N_5O_3S_2$: C, 71.98; H, 8.52; N, 7.50. Found: C, 72.00; H, 8.56; N, 7.39.

*4-(3,4,5-Tris(dodecyloxy)phenyl)-4H-diselenopheno[3,2-b:2′,3′-d]pyrrole (**2b**).* 2,6-Bis(trimethylsilyl)-4-(3,4,5-tris(dodecyloxy)-phenyl)-4*H*-diselenopheno[3,2-*b*:2′,3′-*d*]pyrrole (**1b**) (5.22 mmol, 5.46 g) was dissolved in 25 mL of anhydrous THF and TBAF (1.0 M in THF, 2.2 equiv, 11.48 mmol, 11.5 mL) was added dropwise. The yellow-orange reaction mixture became darker in color. The mixture was stirred for 25 min, analyzed by TLC (hexanes:dichloromethane (2:1) as eluant, consumption of the starting material was confirmed), and the mixture was treated with water (∼20 mL). The dark brown organic phase was separated, the aqueous phase was extracted with hexanes (3 × 15 mL), the combined organic phases were dried over anhydrous magnesium sulfate, and the drying agent was filtered off. The solvent was removed, and the brownish oil was obtained as a crude product (4.01 g, solidified on standing, 85.1% yield, only trace amount of impurity was detected by TLC). This material was purified by column chromatography (silica gel, hexanes:CH_2Cl_2 (2:1), and the yellowish oil was obtained after solvent removal (solidified on standing to give off-white solid). ^{1}H NMR (400 MHz, $CDCl_3$): δ 7.72 (d, J = 5.8 Hz, 2H), 7.40 (d, J = 5.8 Hz, 2H), 6.71 (s, 2H), 4.03 (t, J = 6.6 Hz, 2H), 3.98 (t, J = 6.5 Hz, 4H), 1.81 (m, 6H), 1.49 (m, 6H), 1.40−1.20 (m, 48H), 0.89 (m, 9H). ^{13}C{^{1}H} NMR (400 MHz, $CDCl_3$): δ 153.6, 144.7, 136.8, 135.1, 126.2, 117.9, 115.6, 102.9, 73.6, 69.3, 31.94, 31.92, 30.4, 29.8, 29.69, 29.65, 29.63, 29.40, 29.36, 29.31, 26.14, 26.08, 22.7, 14.1. MS (MALDI-TOF): calcd for $C_{50}H_{81}NO_3Se_2$ 902.5, found 903.5. Anal. Calcd for $C_{50}H_{81}NO_3Se_2$: C, 66.57; H, 9.05; N, 1.55. Found: C, 66.78; H, 9.22; N, 1.60.

*Reaction of **2b** with TCNE.* 4-(3,4,5-Tris(dodecyloxy)phenyl)-4*H*-diselenopheno[3,2-*b*:2′,3′-*d*]pyrrole (**2b**) (2.00 mmol, 1.80 g) and TCNE (4.00 mmol, 1.03 g) were mixed in a flask under nitrogen atmosphere. Anhydrous DMF (25 mL) was added, and the solution became purple within 1 min. The reaction mixture was initially heated to 117 °C and then stirred at 102 °C overnight. The reaction was monitored by TLC in hexanes/dichloromethane (1:1), and after consumption of the starting material the dark blue mixture was cooled to room temperature and treated with water (50 mL). The organic matter was extracted with dichloromethane (four times) and then with chloroform, and combined organic phases were dried over anhydrous magnesium sulfate. The drying agent was filtered off, the organic solvents were removed by rotary evaporation, and the crude product was column chromatographed (silica gel, hexanes:dichloromethane (2:1) as eluant). First fractions containing monosubstituted product **3b** were combined, the solvents were removed by rotary evaporation, and the residue was further purified using prepacked Biotage columns (chloroform as eluant) (0.29 g, 14.6% yield). The next fractions containing disubstituted product **4b** came out with dichloromethane as eluant. The dark blue pure fractions were combined, and the solvents were removed by rotary evaporation to give product as dark blue film, which was further purified using prepacked Biotage columns (chloroform as eluant) (0.99 g, 44%). The next fractions containing slightly contaminated **5b** (dichloromethane as eluant) were combined, the solvents were removed by rotary evaporation, and the residue was further purified by Biotage column chromatography (chloroform as eluant) (0.14 g, 6.9% yield).

3b: ^{1}H NMR (400 MHz, $CDCl_3$): δ 8.23 (m, 2H), 7.35 (d, J = 5.9 Hz, 1H), 6.64 (s, 2H), 4.06 (t, J = 6.5 Hz, 2H), 3.98 (t, J = 6.4 Hz, 4H), 1.84 (m, 6H), 1.49 (m, 6H), 1.26 (m, 48H), 0.90 (m, 9H). ^{13}C{^{1}H} NMR (400 MHz, $CDCl_3$): δ 154.2, 153.8, 145.8, 138.3 (CH), 134.1, 133.5, 132.7, 126.4 (CH), 118.7, 115.5 (CH), 114.0, 113.1, 103.1 (CH), 76.2, 73.8 (CH_2), 69.5 (CH_2), 31.96 (CH_2), 31.93 (CH_2), 30.4 (CH_2), 29.79 (CH_2), 29.77 (CH_2), 29.71 (CH_2), 29.67 (CH_2), 29.64 (CH_2), 29.40 (CH_2), 29.38 (CH_2), 29.3 (CH_2), 26.13 (CH_2), 26.07 (CH_2), 22.7 (CH_2), 14.1 (CH_3) (assignment of the CH, CH_2 and CH_3 carbons was made based on DEPT-135 experiment). HRMS (MALDI-TOF): calcd for ($C_{55}H_{80}N_4O_3Se_2$ + H) 1005.4639, found 1005.4592. Anal. Calcd for $C_{55}H_{80}N_4O_3Se_2$: C, 65.85; H, 8.04; N, 5.58. Found: C, 66.02; H, 8.14; N, 5.43.

4b. ^{1}H NMR (400 MHz, $CDCl_3$): δ 8.28 (s, 2H), 6.63 (s, 2H), 4.08 (t, J = 6.6 Hz, 2H), 3.98 (t, J = 6.4 Hz, 4H), 1.82 (m, 6H), 1.50 (m, 6H), 1.27 (48H), 0.90 (m, 9H). ^{13}C{^{1}H} NMR (400 MHz, $CDCl_3$): δ 154.6, 149.8, 139.5, 139.1, 135.1, 131.3, 128.9, 125.8 (CH), 112.7, 112.5, 111.8, 103.1 (CH), 83.9, 77.4, 77.0, 76.7, 73.9 (CH_2), 69.7 (CH_2), 31.96 (CH_2), 31.93 (CH_2), 30.4 (CH_2), 29.77 (CH_2), 29.72 (CH_2), 29.68 (CH_2), 29.65 (CH_2), 29.41 (CH_2), 29.39 (CH_2), 29.27 (CH_2), 26.12 (CH_2), 26.06 (CH_2), 22.7 (CH_2), 14.1 (CH_3). HRMS (MALDI-TOF): calcd for ($C_{60}H_{79}N_7O_3Se_2$ + H) 1106.4653, found 1106.4667. Anal. Calcd for $C_{60}H_{79}N_7O_3Se_2$: C, 65.26; H, 7.21; N, 8.88. Found: C, 65.34; H, 7.20; N, 8.82 (for material prior to the purification by Biotage column chromatography). Found: C, 65.20; H, 7.12; N, 8.72 (for material after the purification by the Biotage column chromatography).

5b. ^{1}H NMR (400 MHz, $CDCl_3$): δ 6.53 (s, 2H), 6.48 (s, 2H), 4.05 (t, J = 6.6 Hz, 2H), 3.96 (t, J = 6.4 Hz, 4H), 1.82 (m, 6H) 1.49 (m, 6H), 1.27 (m, 48H), 0.89 (t, J = 6.7 Hz, 9H). ^{13}C{^{1}H} NMR (400 MHz, $CDCl_3$): δ 174.5, 165.8, 154.4, 139.5, 131.5, 129.4, 113.7, 112.4, 105.5 (CH), 103.4 (CH), 76.0, 73.8 (CH_2), 69.6 (CH_2), 31.9 (CH_2), 30.4 (CH_2), 29.76 (CH_2), 29.72 (CH_2), 29.69 (CH_2), 29.65 (CH_2), 29.61 (CH_2), 29.38 (CH_2), 29.36 (CH_2), 29.2 (CH_2), 26.0 (CH_2), 22.7 (CH_2), 14.1 (CH_3) (12 alkyl carbon signals are missing due to overlap) (assignment of the CH, CH_2 and CH_3 carbons was made based on DEPT-135 experiment). HRMS (MALDI-TOF): calcd for ($C_{56}H_{79}N_5O_3Se_2$ + H) 1030.4592, found 1030.4478. Anal. Calcd for $C_{56}H_{79}N_5O_3Se_2$: C, 65.42; H, 7.74; N, 6.81. Found: C, 65.55; H, 7.58; N, 6.76.

dx.doi.org/10.1021/jo3020006 | J. Org. Chem. 2012, 77, 10931−10937

■ ASSOCIATED CONTENT

Supporting Information

Computational methodology, table with the summary of the device characterization of **4b**, DSC graphs for the first heating–cooling cycle, HOMO and LUMO (**3**–**5**), and HOMO-1 (**3** and **4**) wave function illustrations, additional micrographs, and tables of atom coordinates and absolute energies for **3**–**5**. This material is available free of charge via the Internet at http://pubs.acs.org

■ AUTHOR INFORMATION

Corresponding Author

*E-mail: seth.marder@chemistry.gatech.edu.

Notes

The authors declare no competing financial interest.

■ ACKNOWLEDGMENTS

This work was supported in part by Solvay S.A., by the STC Program of the National Science Foundation under Agreement No. DMR-0120967. Y.A.G. thanks Benjamin Wunsch for the DSC analyses, Timothy Parker for providing help with the DFT calculations, and Professor John Reynolds for providing access to the microscope equipped with the hot stage.

■ REFERENCES

(1) Jung, B. J.; Tremblay, N. J.; Yeh, M. L.; Katz, H. E. *Chem. Mater.* **2011**, *23*, 568–582.
(2) Anthony, J. E.; Facchetti, A.; Heeney, M.; Marder, S. R.; Zhan, X. W. *Adv. Mater.* **2010**, *22*, 3876–3892.
(3) Brown, A. R.; Deleeuw, D. M.; Lous, E. J.; Havinga, E. E. *Synth. Met.* **1994**, *66*, 257–261.
(4) Yamashita, Y.; Shimono, S.; Kono, T.; Kumaki, D.; Nishida, J.; Tokito, S. *Organic Field-Effect Transistors Vi* **2007**, *6658*, N6580.
(5) El-Nahass, M. M.; Abd-El-Rahman, K. F.; Darwish, A. A. A. *Physica B* **2008**, *403*, 219–223.
(6) Ortiz, R. P.; Facchetti, A.; Marks, T. J.; Casado, J.; Zgierski, M. Z.; Kozaki, M.; Hernandez, V.; Navarrete, J. T. L. *Adv. Funct. Mater.* **2009**, *19*, 386–394.
(7) Bader, M. M.; Pham, P. T. T.; Elandaloussi, E. *Cryst. Growth Des.* **2010**, *10*, 5027–5030.
(8) Zhou, T. L.; Jia, T.; Kang, B. N.; Li, F. H.; Fahlman, M.; Wang, Y. *Adv. Energy Mater.* **2011**, *1*, 431–439.
(9) Hwang, D. K.; Fuentes-Hernandez, C.; Kim, J.; Potscavage, W. J.; Kim, S. J.; Kippelen, B. *Adv. Mater.* **2011**, *23*, 12931298.
(10) Duan, Y. A.; Geng, Y.; Li, H. B.; Tang, X. D.; Jin, J. L.; Su, Z. M. *Org. Electron.* **2012**, *13*, 1213–1222.
(11) Pappenfus, T. M.; Hermanson, B. J.; Helland, T. J.; Lee, G. G. W.; Drew, S. M.; Mann, K. R.; Mcgee, K. A.; Rasmussen, S. C. *Org. Lett.* **2008**, *10*, 1553–1556.
(12) Getmanenko, Y. A.; Tongwa, P.; Timofeeva, T. V.; Marder, S. R. *Org. Lett.* **2010**, *12*, 2136–2139.
(13) Handa, S.; Miyazaki, E.; Takimiya, K.; Kunugi, Y. *J. Am. Chem. Soc.* **2007**, *129*, 11684–11685.
(14) Handa, S.; Miyazaki, E.; Takimiya, K. *Chem. Commun.* **2009**, 3919–3921.
(15) Steckler, T. T.; Zhang, X.; Hwang, J.; Honeyager, R.; Ohira, S.; Zhang, X. H.; Grant, A.; Ellinger, S.; Odom, S. A.; Sweat, D.; Tanner, D. B.; Rinzler, A. G.; Barlow, S.; Bredas, J. L.; Kippelen, B.; Marder, S. R.; Reynolds, J. R. *J. Am. Chem. Soc.* **2009**, *131*, 2824–2826.
(16) Gronowitz, S. *Acta Chem. Scand.* **1961**, *15*, 1393–1395.
(17) Kaplan, M. L.; Haddon, R. C.; Bramwell, F. B.; Wudl, F.; Marshall, J. H.; Cowan, D. O.; Gronowitz, S. *J. Phys. Chem.* **1980**, *84*, 427–431.
(18) Connelly, N. G.; Geiger, W. E. *Chem. Rev.* **1996**, *96*, 877–910.
(19) Pommerehne, J.; Vestweber, H.; Guss, W.; Mahrt, R. F.; Bassler, H.; Porsch, M.; Daub, J. *Adv. Mater.* **1995**, *7*, 551–554.
(20) Burand, M. W.; Mcgee, K. A.; Cai, X. Y.; Da Silva, D. A.; Bredas, J. L.; Frisbie, C. D.; Mann, K. R. *Chem. Phys. Lett.* **2006**, *425*, 251–256.
(21) Faid, K.; Cloutier, R.; Leclerc, M. *Macromolecules* **1993**, *26*, 2501–2507.